ACS Photonics

pubs.acs.org/journal/apchd5

Article

Nonlinear Optical Interactions and Relaxation in 2D Layered Transition Metal Dichalcogenides Probed by Optical and Photoacoustic Z-Scan Methods

Melissa E. Maldonado, Avishek Das, Ali M. Jawaid, Allyson J. Ritter, Richard A. Vaia, Danilo A. Nagaoka, Pilar G. Vianna, Leandro Seixas, Christiano J. S. de Matos, Alexander Baev, Paras N. Prasad,* and Anderson S. L. Gomes*

Cite This: *ACS Photonics* 2020, 7, 3440−3447

Read Online

ACCESS | Metrics & More | Article Recommendations | Supporting Information

ABSTRACT: Atomically thin 2D materials, currently being at the forefront of scientific and technological interest, can be categorized as metallic, semimetallic, semiconducting, insulating, or superconducting, depending on their chemical composition and structural configuration. They also exhibit, in some cases, a transition from an indirect to a direct bandgap alignment when bulk materials are scaled down to monolayers. An important class of 2D materials is layered transition metal dichalcogenides (TMDs) with a tunable bandgap, because photogenerated optical excitations and subsequent excitation dynamics, which produce energy migration and photogenerated charge carrier transport, make them promising candidates for a variety of optoelectronic devices, including solar cells, photodetectors, light-emitting diodes, and phototransistors. In this work, we probe the excitation dynamics following nonlinear optical absorption/scattering in two unexplored TMDs, metallic NbS_2 and semimetallic $ZrTe_2$, using a combination of the standard optical Z-scan and photoacoustic Z-scan techniques, and compare them with semiconducting MoS_2. The comparison of optical Z-scan (OZ-scan), which depends on the contributions of both nonlinear scattering and nonlinear absorption, with photoacoustic Z-scan (PAZ-scan), which depends only on nonlinear absorption due to local heating from nonradiative relaxation, allows us to separate these contributions from the total nonlinear response. In addition, these studies also allow us to look at the nature of nonlinear absorption as to whether it is due to saturable absorption (SA) of a one-photon transition, reverse saturable absorption (RSA) derived from two-photon excitation processes, or any combination thereof. In MoS_2, NbS_2, and $ZrTe_2$, we observed both SA and RSA. The relevant nonlinear absorption coefficient parameters were obtained. Density functional theory modeling provides an insight onto possible underlying physical processes.

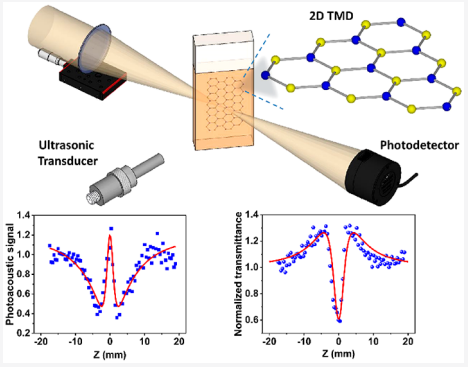

KEYWORDS: *optical Z-scan, photoacoustic Z-scan, TMDs, nonlinear absorption*

Depending on their chemical composition and structural configuration, atomically thin 2D materials can be categorized as metallic, semimetallic, semiconducting, insulating, or superconducting.[1] Semiconducting 2D LTMDs (layered transition metal dichalcogenides) exhibit unique electrical and optical properties that stem from quantum confinement and surface effects that arise during a transition from an indirect bandgap to a direct bandgap, when bulk materials are scaled down to monolayers.[2] This tunable bandgap in semiconducting TMDs is accompanied by a strong photoluminescence (PL) and large exciton binding energy, making them promising candidates for a variety of optoelectronic devices, including solar cells, photodetectors, light-emitting diodes, and phototransistors.[3,4] On the other hand, metallic and semimetallic 2D TMDs have been shown to possess a finite density of states at the Fermi level, which opens up research fields quite distinct from semiconducting materials, as reviewed in ref 1. Generally speaking, TMDs have exceptional optical characteristics: a high refractive index in the visible and IR (n = 4−6); ultrafast carrier dynamics (intraband ∼ fs, interband ∼ ps); a combination of large oscillator strength per unit area ($10^5/nm^2$), large exciton binding energy (∼100 meV), and long lifetimes (>ns); and third-order nonlinearities comparable to graphene and plasmonic nanoparticles ($\mathrm{Im}(\chi^{(3)})/\alpha_0 \sim 1-5 \times 10^{-15}$ esu cm). All these properties are tunable, either by the number of layers in a flake, surface interactions, or lattice strain. The

Received: August 24, 2020
Published: November 9, 2020

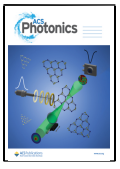

https://dx.doi.org/10.1021/acsphotonics.0c01327
ACS Photonics 2020, 7, 3440−3447

Table 1. Physical Dimensions and NLO Parameters of the 2D TMDs Studied in This Work and Literature Comparison

sample	solvent/ substrate	avg thickness (nm, AFM)	avg lateral extension (nm, TEM)	α (cm^{-1})	scanning type	$\beta \times 10^{-7}$ (cm/W)	I_s (MW/cm^2)
MoS_2, this work	ACN	2.5 ± 1.0	84	2.6	Z-scan	0.53	10
					PAZ	0.20	11.4
MoS_2[27]	PMMA	0.71−3.2	<100	NA	Z-scan	0.62	NA
						0.70	
MoS_2[25]	sapphire	0.67	few square centimeters	NA	Z-scan	-1.01×10^4	370
MoS_2[24]	water/ethanol	2−4	50−400	NA	Z-scan	0.015	NA
NbS_2, this work	ACN	2.0 ± 1.1	121	2.1	Z-scan	0.42	8
					PAZ	0.14	10
$ZrTe_2$, this work	ACN	3.8 ± 1.7	150	1.0	Z-scan	0.5	7
					PAZ	0.24	10.3

combination of several of those properties is quite relevant to the nonlinear optical (NLO) properties of 2D TMDs, which have been well studied in their semiconducting form,[4] but not as much in metallic and semimetallic structures.

Among several NLO techniques employed to characterize nonlinear photonic materials, both in bulk and nanostructured forms, optical Z-scan (OZ-scan)[5,6] and, more recently, photoacoustic Z-scan (PAZ-scan)[7−9] have been employed, giving rise to information on nonlinear refraction, nonlinear absorption, and nonlinear scattering.

In this Article, we report on the nonlinear absorption (NLA) properties of three different TMDs in suspension, namely, the semiconducting MoS_2, metallic NbS_2, and semimetallic $ZrTe_2$ dispersed in acetonitrile. The samples were synthesized using the redox exfoliation method.[10] In a 2018 report by Tsipas et al.,[11] thin film semimetallic (2D single and few layers) 1T phase $ZrTe_2$ prepared by molecular beam epitaxy were grown on InAs and morphologically characterized. Theoretical calculations confirmed the semimetallic character, with the bands crossing at a point near the Fermi level, which indicates massless 3D Dirac Fermions, characteristic of a topological Dirac semimetal behavior.[11] As for 2D NbS_2, the growth, linear optics, and transport studies have been performed and reported by Zhao and co-workers,[12] with the atomic few layers (3R phase in their case) grown by chemical vapor deposition on hexagonal boron nitride, whereby they verified that since their sample was three layers thick, it behaved as a metallic LTMD. The present studies of the NLA in three different 2D LTMD nanoflakes were carried out using an optical and photoacoustic Z-scan (PAZ-scan) setup at a 532 nm wavelength and in the nanosecond regime. While MoS_2 has been widely studied, this is not the case for the 2H phase NbS_2 and 1T phase $ZrTe_2$, whose NLA properties in the nanosecond regime are reported here for the first time.

EXPERIMENTAL DETAILS

Sample Preparation. All samples were synthesized by the redox exfoliation method, whose preparation details and characterization confirming monolayer-enriched dispersions were reported in ref 10. For completeness, we summarize here the main aspects of the synthesis, highlighting MoS_2, as an example. The redox exfoliation of TMD powders from group IV, V, VI, and VII materials were basically carried out by sequential surface oxidation and reduction reactions with a weak organic hydroperoxide and an inorganic reducing agent, respectively. The synthesis starts with a suspension of bulk TMD powder in acetonitrile solvent, followed by weak oxidation treatment, which results in the formation of a peroxometalate precursor and unexfoliated TMD sedimentation. The subsequent addition of a reducing agent in the solution triggers the formation of anionic polyoxometalates (POMs). Such POMs are adsorbed to the basal surface of TMDs, thereby creating a Coulombic repulsion force to facilitate exfoliation down to single to few-layer thicknesses.

Surface Oxidation. Prior to synthesizing 2D TMDs, the round-bottom flasks were cleaned and an inert environment was maintained in order to minimize side reactions. Initially, bulk MoS_2 powder of 0.625 mmol suspended in 5 mL of acetonitrile (CH_3CN, ACN) was added into the flask and stirred at 0 °C over an ice bath for 30 min. After reaching thermal equilibrium, a mixture of 3 mmol of cumenehydroperoxide (80% CHP) and 5 mL of ACN was introduced dropwise into the previously prepared MoS_2 suspension for every 15 min under constant stirring at 0 °C. After the complete addition of CHP, the bath solution was stirred at 25 °C for 24 h. Similar process recipes were followed for the surface oxidation of NbS_2 and $ZrTe_2$.

Exfoliation. After the settlement of the MoS_2 powder at the bottom of the flask, the oxidized solution volume was reduced to 4 mL and stirred at 0 °C for 30 min. After reaching equilibrium, 50 μL of aqueous solution of 100 mM $NaBH_4$ was instantly introduced into the above oxidized solution and kept under constant stirring for 1 h. The process was repeated a few times to increase the solution volume. The solution was stirred at room temperature for 24 h and allowed to settle down the unexfoliated flakes. Later, the supernatant was isolated, centrifuged at 10000 rpm for 15 min to sediment the exfoliated flakes. Finally, the exfoliated monolayer MoS_2 flakes are obtained with successive sedimentation and redispersion in fresh anhydrous ACN. Similar process recipes were followed for the exfoliation of NbS_2 and $ZrTe_2$.[10]

Exfoliated monolayer TMD samples were isolated for morphological and structural characterizations by employing SEM, AFM, TEM, and XRD (see ref 10 and Supporting Information therein). The summarized average thickness and lateral size of flakes in the dispersion are provided in Table 1.

Optical Absorption. Linear absorbance spectra were acquired with a Cary 5000 UV−vis-NIR spectrophotometer for the few-layer suspensions of MoS_2, NbS_2, and $ZrTe_2$ in acetonitrile, as shown in Figure 1.

One can observe the characteristic absorption peaks for MoS_2 (blue line) in the 600−700 nm range; these peaks are known as the B and A transitions and indicate that MoS_2 is in the phase 2H.[13,14] Furthermore, the MoS_2 has a broad absorption band at 400−500 nm, known as the C transition. The NbS_2 and the $ZrTe_2$ have strong absorption in the UV

https://dx.doi.org/10.1021/acsphotonics.0c01327
ACS Photonics 2020, 7, 3440−3447

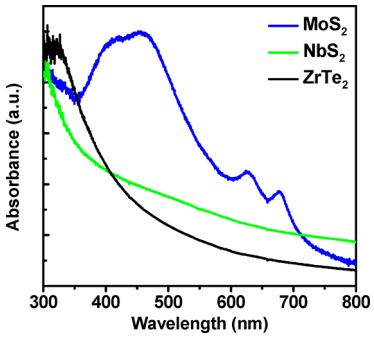

Figure 1. Linear absorption spectra for the samples: blue, MoS_2; green, NbS_2; black, $ZrTe_2$.

region, remaining largely featureless within the visible spectral range, which is compatible with their metallic and semimetallic natures.

Raman Characterization. Further characterization of the three samples by Raman spectra is shown in Figure 2. It is

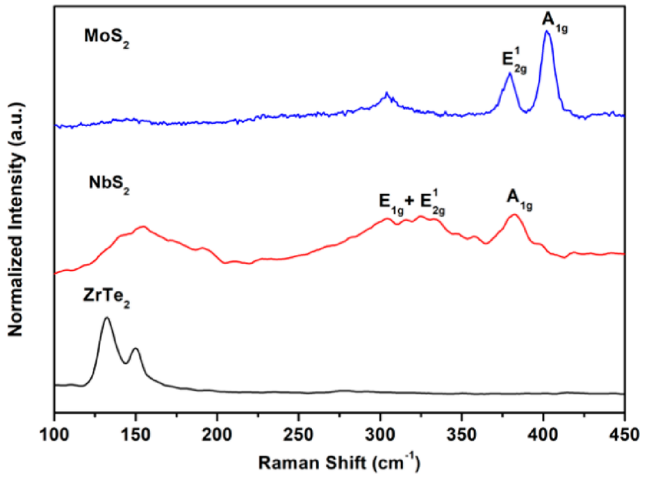

Figure 2. Raman spectra of drop-casted samples of MoS_2 (blue), NbS_2 (red), and $ZrTe_2$ (black).

worth noting that the Raman characterization of exfoliated few-layer metallic NbS_2 and semimetallic $ZrTe_2$ is rarely reported in the literature. In one of the few examples, the Raman spectra for NbS_2 in 3R phase prepared by mechanical exfoliation and found to exhibit a semiconducting character was reported in ref 15.

For the present measurements, the exfoliated TMD suspensions were drop-casted on a silicon substrate and dried before measurement. Note that bare NbS_2 and $ZrTe_2$ flakes are highly susceptible to oxidation, thus, drop-casting and measurements for these samples were carried out under a nitrogen purge.

Optical and Photoacoustic Z-Scan Setup. The experimental setup for the OZ- and PAZ-scans is shown in Figure 3. The optical source for the experiment was an optical parametric oscillator (OPO) operating at 532 nm, 10 Hz with pulses of 5 ns.

The beam was transmitted through two Glan polarizers for controlling the incident power; after that, a telescope setup was used to increase the beam diameter by a factor 2. A beam splitter directed a part of the beam to a reference photodetector (PD1), for input power measurements, while the

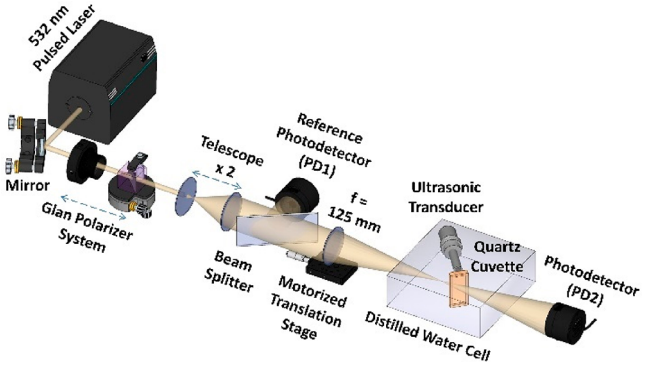

Figure 3. Experimental setup used for measuring simultaneously the open aperture OZ-scan and PAZ-scan.

remaining of the beam was focused onto the sample with a 125 mm focal length lens. The lens was placed on a motorized translational stage and moved in small steps such that the focal region of the beam scanned the sample along the z-direction. The sample was placed in a 2 mm quartz cuvette at 45 deg and mounted in a cell containing distilled water for ultrasound coupling. The PA signal was detected using a 10 MHz water immersion transducer (Olympus V312-N-SU) in front of the sample surface for better coupling. The transmitted beam was collected by a photodetector (PD2) for open aperture OZ-scan measurements. The beam radius at the focus ($z = 0$) was $w_0 = 18\ \mu$m.

RESULTS AND DISCUSSION

We first analyze and discuss the Raman spectra in Figure 2. The MoS_2 spectrum shows the characteristic $E_{2g}{}^1$ and A_{1g} Raman peaks at 379 and 402 cm^{-1}, respectively. The frequency difference between these peaks depends on the number of layers per stack; 23 cm^{-1} is consistent with single to few-layer MoS_2.[16] The NbS_2 sample exhibits a peak at 382 cm^{-1}, assigned to the A_{1g} mode, and a broad peak at ~320 cm^{-1}, which is believed to be a composition of the E_{1g} and $E_{2g}{}^1$ modes.[17] A third, broad peak at ~160 cm^{-1} has not been assigned but has been recently observed in NbS_2 samples grown by chemical vapor deposition.[17] Finally, the $ZrTe_2$ sample exhibits two unassigned peaks at 132 and 153 cm^{-1}. Although, to the best of our knowledge, the Raman spectrum of a few-layer $ZrTe_2$ has not been experimentally reported, bulk samples present the E_g and A_{1g} modes at 104 and 145 cm^{-1}, respectively.[18] Further characterization would be required to relate the observed peaks with these modes. Nevertheless, the observation of well-defined peaks assigned to NbS_2 and $ZrTe_2$ confirms that acetonitrile successfully prevents the oxidation and degradation of these materials even in the few-layer form. Indeed, even under nitrogen purge, the Raman signal of dried NbS_2 samples was found to degrade over a time interval of minutes.

For the nonlinear absorption study, the OZ and PAZ-scan measurements were first carried out with the MoS_2 suspension, which is the most studied TMD in the literature. Figures 4(a,b) show the normalized transmittance traces obtained by OZ-scan for increasing intensities. In Figure 4a, for a lower intensity (0.12 GW/cm^2), the normalized transmission curve for OZ-scan shows an increase in transmittance near the focus ($z = 0$), indicating that a SA mechanism dominates. However, even at this intensity, a small dip can be observed at $z = 0$, which points to a change in the dynamics at higher intensities.

https://dx.doi.org/10.1021/acsphotonics.0c01327
ACS Photonics 2020, 7, 3440−3447

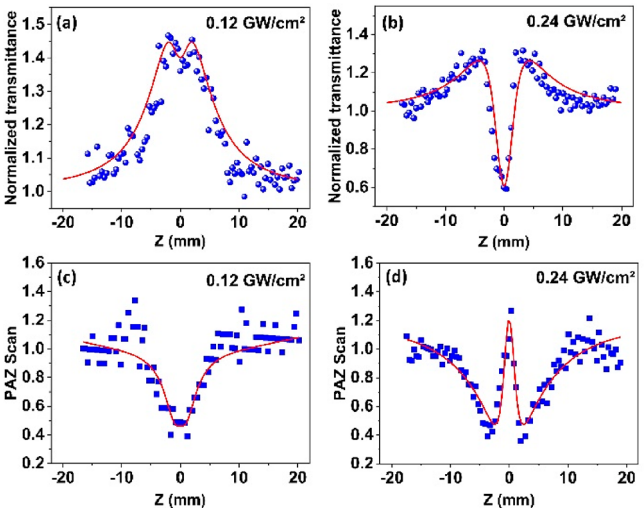

Figure 4. OZ and PAZ-scan results for MoS_2. (a, b) Open aperture optical Z-scan signatures for different intensities. (c, d) Respective photoacoustic Z-scan signatures.

As the incident intensity increases (0.24 GW/cm^2 in Figure 4b), a valley inside the peak at the focus appears, the amplitude of which increases gradually, indicating the rise of a RSA behavior. Typically, RSA can be a sign of nonlinear scattering (NLS) or nonlinear intensity dependent absorption by direct two-photon absorption (2PA) or due to absorption by photogenerated species (PSA), such as free carriers (FCA). The NLA and NLS processes, nevertheless, have quite different PAZ-scan signatures. Figure 4c,d shows the photoacoustic signals obtained by a PAZ-scan with the same intensities. We can observe that the PAZ-scan appears to be a mirror image of the optical Z-scan (i.e., with curves reflected in a horizontal mirror), which is a good indicator that nonlinear absorption (2PA and PSA), rather than nonlinear scattering, dominates in the 2D MoS_2 nanoflakes suspension at these higher intensities.

In order to quantitatively characterize nonlinear attenuation via both OZ-scan and PAZ-scan, a simple optical nonlinearity model was used to fit the experimental data (red lines in Figure 4), which helps provide physical insight. To account for SA and RSA in the third-order nonlinearity, $\chi^{(3)}$, the absorption coefficient was assumed to be given by[19,20]

$$\alpha(I) = \frac{\alpha_0}{1 + \frac{I(z)}{I_s}} + \beta I(z) \tag{1}$$

where $I(z) = {I_0}/{(1 + {z^2}/{z_0^2})}$ is the optical intensity, z_0 is the beam's diffraction length, α_0 is the linear absorption coefficient, I_s is the saturation intensity, and β is the nonlinear attenuation coefficient, which can in principle include absorption mechanisms, such as 2PA and free carrier absorption (FCA), and nonlinear scattering. Light intensity within the sample then evolves along the optical axis, z, according to

$$\frac{dI}{dz'} = -\alpha(I)I \tag{2}$$

which was then numerically integrated[21] over the sample thickness and the cross-sectional area of the laser beam to find the transmitted power as in eq 3. This provides a best fit to the OZ-scan data, with the free parameters in eq 1 (see Supporting Information).

$$P_{out}(z) = P_{in}(z) - 2\pi \int_0^{\infty} \int_{-L/2}^{L/2} r \left(\frac{\alpha_0 I(z', z, r)}{1 + I(z', z, r)/I_{sat} + \beta I^2(z', z, r)} \right) dz'\, dr \tag{3}$$

We also performed a fit to the experimental data using an approximate equation following refs 5 and 21, and the comparison showed very little discrepancy (see Supporting Information, where the details of the numerical integration are also given).

In the PAZ-scan, the acoustic signal amplitude P is proportional to the absorption coefficient $\alpha(I)$, that is, $P(z) = \Gamma\alpha(I)I(z)$, where Γ is the Grüneisen coefficient, which depends on the material properties and the laser beam characteristics.[7,9] Using eq 1 and normalizing the photoacoustic signal relative to its linear absorption expression,[8,9] one gets

$$P_N(z) = \frac{I_s}{I_s + I(z)} + \frac{\beta}{\alpha_0} I(z) \tag{4}$$

The numerical integration from eq 1, which is more rigorous in comparison to the usual approximations, was used to fit (red lines) the OZ-scan data (blue dots) in Figure 4a,b, while the fit to eq 4 was used for the data in Figures 4c,d. Note that the PA signal is insensitive to scattering processes; thus, we can expect that the PAZ-scan measurements only detect absorptive processes. Significant discrepancies between the nonlinear optical parameters obtained from the two measurements (OZ-scan and PAZ-scan) can then be attributed to nonlinear scattering or to absorptions, followed by radiative decays. Table 1 shows the nonlinear optical parameters obtained by both OZ-scan and PAZ-scan for MoS_2.

In the literature, SA followed by RSA as the intensity increases, has been reported for few layers of MoS_2 at 532 nm, with pulses of a few ns.[22−25] However, in ref 22, the RSA behavior was attributed to nonlinear scattering (which was experimentally confirmed), and in ref 23, it was partly attributed to nonlinear scattering (and partly to free carrier absorption, FCA), whereas in refs 24 and 25, it is attributed to FCA. In particular, ref 26 reports PAZ-scan measurements in MoS_2, where nonlinear scattering did not seem to play a significant role, although no quantitative values are reported from the photoacoustic data.

In ref 26, picosecond pulses at 532 nm were used, and either SA or RSA was observed, depending on the average flake thickness; both 2PA and excited state absorption were suggested as RSA mechanisms. We note that the emergence of nonlinear scattering is expected to be highly dependent on the TMD concentration, thickness, and on the used solvent. Therefore, it is difficult to compare the different results reported in the literature. In addition, we need to keep in mind that 2PA is an instantaneous nonlinear effect that requires a high-power density to ensure the interaction between two photons and an electron.

On the other hand, PSA produces a cumulative nonlinear effect that depends on the accumulation of the excited species population; that means, for long pulse width, PSA effects can occur even at relatively low intensities. In the nanosecond regime, the nonlinearity is dominated by PSA, but if the laser intensity is high enough, the effect of 2PA may also appear. From the current results, it is difficult to determine if the photogenerated species giving rise to excited state linear

https://dx.doi.org/10.1021/acsphotonics.0c01327
ACS Photonics 2020, 7, 3440−3447

absorption contribution to RSA are hot free carriers, relaxed free carriers, or recombined excitons, especially in view of the long pulse durations. Only a knowledge of carrier lifetime can provide insight into this. Our experimental results for MoS_2 confirm other literature data in the same spectro-temporal regime. However, the role of scattering cannot be ruled out, since $\beta_{OZ\text{-}scan} > \beta_{PAZ\text{-}scan}$ by a factor of 2.65, and therefore, other loss mechanisms must be taken into account. We added in Table 1, the values for the NLA from refs 24, 25, and 27, which were obtained for MoS_2 at 532 nm with nanosecond pulses. For MoS_2 in PMMA,[27] it is of the same order of magnitude as reported herein. From the work of ref 24, MoS_2 in water/ethanol, the NLA was 1 order of magnitude smaller. However, from ref 25, the NLA for MoS_2 on sapphire is 4 orders of magnitude higher. Thus, these values vary with the environment and MoS_2 morphology, necessitating future studies that systematically examine these factors.

Let us now turn to the two least studied TMDs. 2D NbS_2 nanoflakes, which are metallic TMDs, are very attractive due to their exotic properties.[28,29] The bulk is a superconductor but does not present charge-density waves (CDW) formation. In few-layer thicknesses, metallic transport properties are reported. It has two stable phases at room temperature: 2H- and 3R-NbS_2, which become the same phase in the monolayer limit; for multilayer crystals, their difference is on the layer stacking. This different stacking leads to different physical properties. In this study, the 2H-NbS_2 phase is present, and this is demonstrated in the TEM and Raman analysis in recent studies.[30]

Figure 5a,b shows the OZ-scan normalized transmittance, and Figure 5c,d shows the normalized PAZ-scan signal for the

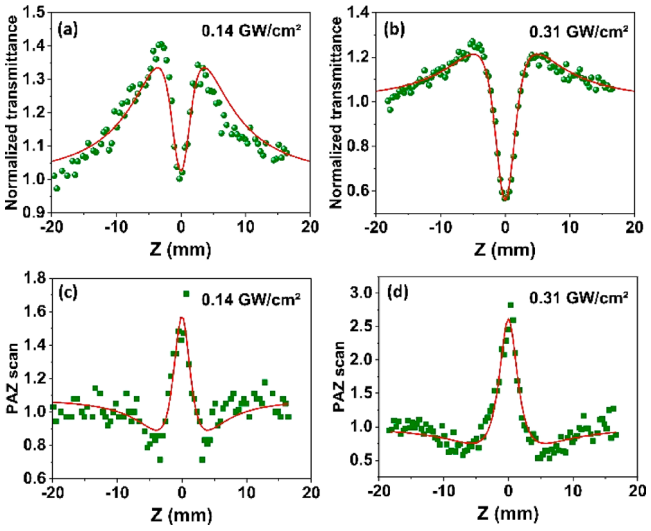

Figure 5. OPAZ-scan results for NbS_2. (a, b) Open Z-scan signatures for different intensities. (c, d) Respective photoacoustic Z-scan signatures.

NbS_2 suspension for two different intensities. The overall nonlinear absorption behavior is similar to that of MoS_2, with both SA and RSA observed. However, in this case, even for the lower intensity, RSA is already present. When we increase the intensity, the amplitude of the valley at the focus also increased and, eventually, RSA dominates. Calculations were performed as described before, and the results in Table 1 follow the same conclusion as in MoS_2, with nonlinear scattering also playing a role in nonlinear transmission (NLT). In this case, $\beta_{OZ\text{-}scan} = 3\beta_{PAZ\text{-}scan}$ and the contribution of NLS to the NLT is slightly higher than in MoS_2. It should be noticed that the NLS mechanism was also observed to contribute to the NLT process for the same NbS_2 sample studied by 800 nm optical Z-scan with 100 fs input pulses.[30]

$ZrTe_2$ presents a semimetallic character, as confirmed recently via angle-resolved photoemission spectroscopy (ARPES),[11] besides its topological semimetal character.[31] Figure 6 shows the results for OZ- and PAZ-scans. Notice

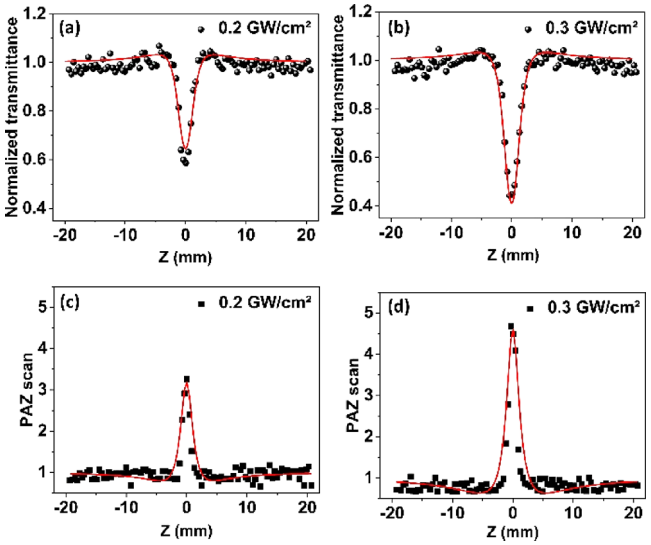

Figure 6. OZ-scan and PAZ-scan signatures for $ZrTe_2$. (a, b) Open Z-scan signatures for different intensities. (c, d) Respective photoacoustic Z-scan signatures.

that, in this case, we observed a significant decrease in transmittance at the focus even at the lowest intensity, for OZ-scan, which is mirror-reflected in the PAZ-scan. These features clearly show that nonlinear attenuation in $ZrTe_2$ is dominated by RSA in the investigated intensity range. However, the fitting parameters, presented in Table 1, reveal that SA also takes place.

The RSA dominance is attributed to the lower linear absorption coefficient, α_0, when compared to that of MoS_2 and NbS_2. The role of NLS is also present for $ZrTe_2$, with $\beta_{OZ\text{-}scan} = 2.08\beta_{PAZ\text{-}scan}$, as can be seen from the values of β in Table 1.

In order to obtain some additional physical insight into the absorptive processes involved in the nonlinear absorption of NbS_2 and $ZrTe_2$, the Density Functional Theory (DFT) simulations[32,33] were carried out using the SIESTA code.[34] The Kohn−Sham orbitals were calculated with a linear combination of atomic orbitals (LCAO) with localized double-ζ basis (DZP) parametrization. The basis range was set by the energy shift of 0.03 eV. We use mesh cutoff of 400 Ry, norm-conserved pseudopotentials with Troullier−Martins parametrization,[35] and k-points sampling with Monkhorst−Pack algorithm with 20 × 20 × 1 grid.[36] For the exchange-correlation functional, we use the Vydrov−van Voorhis functional (vdW-VV),[37] which includes nonlocal terms for the correction of van der Waals forces. All geometries were completely relaxed until forces less than 0.001 eV/Å.

In Figure 7, we show the electronic band structures of NbS_2 and $ZrTe_2$ monolayers, as well as some of the possible optical (vertical) transitions for 2.33 eV photon energy (correspond-

https://dx.doi.org/10.1021/acsphotonics.0c01327
ACS Photonics 2020, 7, 3440−3447

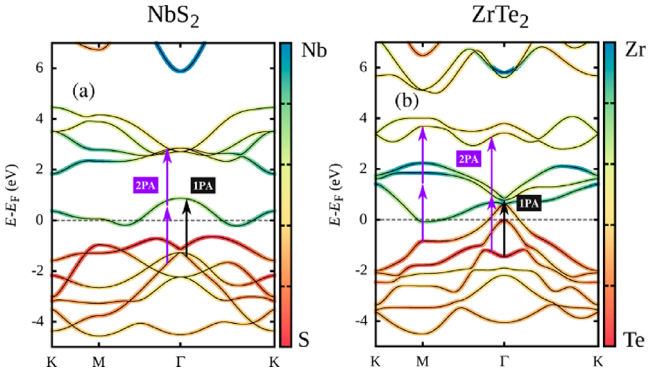

Figure 7. Electronic band structure and optical vertical transitions for one-photon absorption and two-photon absorption at 532 nm: (a) NbS_2 monolayer; (b) $ZrTe_2$ monolayer.

ing to the 532 nm wavelength). The band structure was decomposed by atomic orbitals from the transition metal (Nb or Zr) and chalcogen (S or Te) atoms. These contributions were calculated from the coefficients of the LCAO basis. The transition metal contributions are shown in blue, while the chalcogen contributions are shown in red. NbS_2 is a metal with the Fermi level at a band corresponding to an electron wave function with a predominant overlap with Nb atoms; $ZrTe_2$ is a semimetal with a hole pocket close to the Γ point and electron pockets close to the M points. The shown optical transitions are those connecting the bands at points as close as possible to plateaus representing a van hove singularity, as these are expected to present higher oscillator strengths. For one-photon absorption (1PA), we show optical transitions from chalcogen *p* orbitals to transition metal *d* orbitals, shown as black arrows in Figure 7. For 2PA, we show optical transitions between orbitals of similar character, following the proper selection rules for 2PA. These 2PA transitions are shown as purple arrows in the Figure.

Considering that the oscillator strength of transitions increases when they take place at *k*-space points where the bands have a vanishing gradient and thus van hove singularities, we can see that for NbS_2, 1PA near the Γ point can be significant, and may be the origin of both SA and PSA, with the latter leading to RSA. At a higher intensity, 2PA may also play a role in the RSA mechanism, since it involves a near-zero-gradient point for the excited state. In the case of $ZrTe_2$, 1PA plays a role, as the shown black arrow connects band points near plateaus. However, the fact that the plateau in the valence band corresponds to a local minimum (rather than a maximum) means that the density of states (DoS) in not as high, which may explain the relatively low linear absorption coefficient (and, thus, reduced SA). In contrast, for 2PA, a van Hove singularity (VHS) near the Γ point leads to a peak in DoS, explaining its β value, comparable to MoS_2 and NbS_2. The calculated DoS is shown in the Supporting Information.

Our present data and their analysis are clearly suggestive of possible nonlinear absorption processes. However, to fully establish the exact nature of RSA, we plan to conduct time-resolved pump−probe experiments and a more detailed theoretical modeling to include all possible one- and two-photon vertical transitions (both resonant and nonresonant with energy bands) across the whole first Brillouin zone. Also, further physical insight would be obtained by measurements at various pump wavelengths, in which case theoretically matching particular spectral features could be attempted. Our fitting method does not include a quadratic term in intensity in eq 1, which neglects excited state absorption originating from a two-photon absorption event. However, the good obtained fittings using eq 1 indicate that this nonlinear process is not dominant in the studied intensity range.

CONCLUSIONS

We have reported on the excitation dynamics following nonlinear optical absorption/scattering in two important TMDs nanoflakes, metallic NbS_2 and semimetallic $ZrTe_2$, and compared them with semiconducting MoS_2 using a combination of the standard optical Z-scan and photoacoustic Z-scan. While MoS_2 has been well described in the literature and our results corroborate the findings, NbS_2 and $ZrTe_2$ have their NLA properties at 532 nm reported here for the first time. In the spectro-temporal regime studied, the role of nonlinear scattering was distinguished from the nonlinear absorption, thanks to the simultaneous use of optical and photoacoustic Z-scan techniques. The values of the NLA coefficients were numerically obtained from the experimental data. The NLA mechanisms in both materials were qualitatively analyzed based on DFT simulations. As the 2D LTMDs family of nanomaterials are being used for important technological applications, the fundamental results reported here will be useful in the design of photonics devices.

ASSOCIATED CONTENT

Supporting Information

The Supporting Information is available free of charge at https://pubs.acs.org/doi/10.1021/acsphotonics.0c01327.

The numerical integration steps for the Z-scan fittings are detailed, followed by the density of states (DOS) results from the DFT calculations (PDF)

AUTHOR INFORMATION

Corresponding Authors

Anderson S. L. Gomes − *Departamento de Física, Universidade Federal de Pernambuco, Recife, PE 50670-901, Brazil;* orcid.org/0000-0001-6536-6570; Email: anderson.lgomes@ufpe.br

Paras N. Prasad − *Institute for Lasers, Photonics, and Biophotonics and The Department of Chemistry, University at Buffalo, The State University of New York, Buffalo, New York 14260, United States;* orcid.org/0000-0002-0905-7084; Email: pnprasad@buffalo.edu

Authors

Melissa E. Maldonado − *Departamento de Física, Universidade Federal de Pernambuco, Recife, PE 50670-901, Brazil*

Avishek Das − *Departamento de Física, Universidade Federal de Pernambuco, Recife, PE 50670-901, Brazil*

Ali M. Jawaid − *Materials and Manufacturing Directorate, AFRL, Wright-Patterson Air Force Base, Dayton, Ohio, United States*

Allyson J. Ritter − *Materials and Manufacturing Directorate, AFRL, Wright-Patterson Air Force Base, Dayton, Ohio, United States*

Richard A. Vaia − *Materials and Manufacturing Directorate, AFRL, Wright-Patterson Air Force Base, Dayton, Ohio, United States;* orcid.org/0000-0003-4589-3423

https://dx.doi.org/10.1021/acsphotonics.0c01327
ACS Photonics 2020, 7, 3440−3447

Danilo A. Nagaoka − *MackGraphe, Universidade Presbiteriana Mackenzie, 01302-907 São Paulo-SP, Brazil*
Pilar G. Vianna − *MackGraphe, Universidade Presbiteriana Mackenzie, 01302-907 São Paulo-SP, Brazil;* orcid.org/0000-0001-9767-5538
Leandro Seixas − *MackGraphe, Universidade Presbiteriana Mackenzie, 01302-907 São Paulo-SP, Brazil;* orcid.org/0000-0001-7420-0708
Christiano J. S. de Matos − *MackGraphe, Universidade Presbiteriana Mackenzie, 01302-907 São Paulo-SP, Brazil*
Alexander Baev − *Institute for Lasers, Photonics, and Biophotonics and The Department of Chemistry, University at Buffalo, The State University of New York, Buffalo, New York 14260, United States*

Complete contact information is available at: https://pubs.acs.org/10.1021/acsphotonics.0c01327

Author Contributions

The manuscript was written through contributions of all authors.

Funding

The authors thank the financial support from CAPES and FACEPE. A.S.L.G., C.J.S.d.M., and M.M. acknowledge support from AFOSR. C.J.S.d.M. acknowledges support from FAPESP (Thematic Projects Nos. 2015/11779-4 and 2018/25339-4), the Brazilian Nanocarbon Institute of Science and Technology (INCT/Nanocarbono), and CAPES − PRINT (Programa Institucional de Internacionalização; Grant No. 88887.310281/2018-00). L.S. acknowledges financial support of CNPq (Grant No. 408525/2018-5) and high-performance computing facilities of NACAD/COPPE, UFRJ. P.G.V. and D.A.N. are supported by CAPES scholarships. The work at the Institute for Lasers, Photonics and Biophotonics at the University at Buffalo was also partially supported by funds provided by the office of Vice President for research and economic development.

Notes

The authors declare no competing financial interest.

■ ACKNOWLEDGMENTS

The research reported here was supported by the Air Force Office of Scientific Research. The authors are very thankful to Prof. Marek Samoc, from Wrocław University of Science and Technology, for very useful discussions and insights on the present results.

■ REFERENCES

(1) Han, G. H.; Duong, D. L.; Keum, D. H.; Yun, S. J.; Lee, Y. H. Van Der Waals Metallic Transition Metal Dichalcogenides. *Chem. Rev.* **2018**, *118* (13), 6297−6336.
(2) Choi, W.; Choudhary, N.; Han, G. H.; Park, J.; Akinwande, D.; Lee, Y. H. Recent Development of Two-Dimensional Transition Metal Dichalcogenides and Their Applications. *Mater. Today* **2017**, *20* (3), 116−130.
(3) Huo, N.; Yang, Y.; Li, J. Optoelectronics Based on 2D TMDs and Heterostructures. *J. Semicond.* **2017**, *38* (3), 031002.
(4) Autere, A.; Jussila, H.; Dai, Y.; Wang, Y.; Lipsanen, H.; Sun, Z. Nonlinear Optics with 2D Layered Materials. *Adv. Mater.* **2018**, *30* (24), 1705963.
(5) Sheik-Bahae, M.; Said, A. A.; Wei, T.-H.; Hagan, D. J.; Van Stryland, E. W. Sensitive Measurement of Optical Nonlinearities Using a Single Beam. *IEEE J. Quantum Electron.* **1990**, *26* (4), 760−769.
(6) de Araújo, C. B.; Gomes, A. S. L.; Boudebs, G. Techniques for Nonlinear Optical Characterization of Materials: A Review. *Rep. Prog. Phys.* **2016**, *79* (3), 036401.
(7) Yelleswarapu, C. S.; Kothapalli, S.-R. Nonlinear Photoacoustics for Measuring the Nonlinear Optical Absorption Coefficient. *Opt. Express* **2010**, *18* (9), 9020.
(8) Chantharasupawong, P.; Philip, R.; Thomas, J. Simultaneous Optical and Photoacoustic Measurement of Nonlinear Absorption. *Appl. Phys. Lett.* **2013**, *102* (4), 041116.
(9) Kislyakov, I. M.; Yelleswarapu, C. S. Nonlinear Scattering Studies of Carbon Black Suspensions Using Photoacoustic Z-Scan Technique. *Appl. Phys. Lett.* **2013**, *103* (15), 151104.
(10) Jawaid, A. M.; Ritter, A. J.; Vaia, R. A. Mechanism for Redox Exfoliation of Layered Transition Metal Dichalcogenides. *Chem. Mater.* **2020**, *32* (15), 6550−6565.
(11) Tsipas, P.; Tsoutsou, D.; Fragkos, S.; Sant, R.; Alvarez, C.; Okuno, H.; Renaud, G.; Alcotte, R.; Baron, T.; Dimoulas, A. Massless Dirac Fermions in $ZrTe_2$ Semimetal Grown on InAs (111) by van Der Waals Epitaxy. *ACS Nano* **2018**, *12* (2), 1696−1703.
(12) Zhao, S.; Hotta, T.; Koretsune, T.; Watanabe, K.; Taniguchi, T.; Sugawara, K.; Takahashi, T.; Shinohara, H.; Kitaura, R. Two-Dimensional Metallic NbS_2: Growth, Optical Identification and Transport Properties. *2D Mater.* **2016**, *3* (2), 025027.
(13) Maldonado, M.; da Silva Neto, M. L.; Vianna, P. G.; Ribeiro, H. B.; Martinho, L. M.; Germano, G. C. M.; Carvalho, I. C. S.; de S. Menezes, L.; de Araújo, C. B.; de Matos, C. J. S.; Jawaid, A. M.; Ritter, A. J.; Vaia, R. A.; Gomes, A. S. L. Nonlinear Absorption and Optical Limiting Effect in Redox Exfoliated Layered Transition Metal Dichalcogenides. *Latin America Optics and Photonics Conference*; OSA: Washington, D.C., 2018; p W4E.3.
(14) Manzeli, S.; Ovchinnikov, D.; Pasquier, D.; Yazyev, O. V.; Kis, A. 2D Transition Metal Dichalcogenides. *Nat. Rev. Mater.* **2017**, *2* (8), 17033.
(15) Huang, Y. H.; Peng, C. C.; Chen, R. S.; Huang, Y. S.; Ho, C. H. Transport Properties in Semiconducting NbS_2 Nanoflakes. *Appl. Phys. Lett.* **2014**, *105* (9), 093106.
(16) Han, S. A.; Bhatia, R.; Kim, S.-W. Synthesis, Properties and Potential Applications of Two-Dimensional Transition Metal Dichalcogenides. *Nano Converg.* **2015**, *2* (1), 17.
(17) Yang, J.; Mohmad, A. R.; Wang, Y.; Fullon, R.; Song, X.; Zhao, F.; Bozkurt, I.; Augustin, M.; Santos, E. J. G.; Shin, H. S.; Zhang, W.; Voiry, D.; Jeong, H. Y.; Chhowalla, M. Ultrahigh-Current-Density Niobium Disulfide Catalysts for Hydrogen Evolution. *Nat. Mater.* **2019**, *18* (12), 1309−1314.
(18) Hangyo, M.; Nakashima, S.-I.; Mitsuishi, A. Raman Spectroscopic Studies of MX_2-Type Layered Compounds. *Ferroelectrics* **1983**, *52* (1), 151−159.
(19) Varma, S. J.; Kumar, J.; Liu, Y.; Layne, K.; Wu, J.; Liang, C.; Nakanishi, Y.; Aliyan, A.; Yang, W.; Ajayan, P. M.; Thomas, J. 2D TiS 2 Layers: A Superior Nonlinear Optical Limiting Material. *Adv. Opt. Mater.* **2017**, *5* (24), 1700713.
(20) Wang, K.; Wang, J.; Fan, J.; Lotya, M.; O'Neill, A.; Fox, D.; Feng, Y.; Zhang, X.; Jiang, B.; Zhao, Q.; Zhang, H.; Coleman, J. N.; Zhang, L.; Blau, W. J. Ultrafast Saturable Absorption of Two-Dimensional MoS_2 Nanosheets. *ACS Nano* **2013**, *7* (10), 9260−9267.
(21) Kurian, P. A.; Vijayan, C.; Sathiyamoorthy, K.; Suchand Sandeep, C. S.; Philip, R. Excitonic Transitions and Off-Resonant Optical Limiting in CdS Quantum Dots Stabilized in a Synthetic Glue Matrix. *Nanoscale Res. Lett.* **2007**, *2* (11), 561−568.
(22) Zhang, H.; Lu, S. B.; Zheng, J.; Du, J.; Wen, S. C.; Tang, D. Y.; Loh, K. P. Molybdenum Disulfide (MoS_2) as a Broadband Saturable Absorber for Ultra-Fast Photonics. *Opt. Express* **2014**, *22* (6), 7249.
(23) Dong, N.; Li, Y.; Feng, Y.; Zhang, S.; Zhang, X.; Chang, C.; Fan, J.; Zhang, L.; Wang, J. Optical Limiting and Theoretical Modelling of Layered Transition Metal Dichalcogenide Nanosheets. *Sci. Rep.* **2015**, *5* (1), 14646.
(24) Zhao, M.; Chang, M.-J.; Wang, Q.; Zhu, Z.-T.; Zhai, X.-P.; Zirak, M.; Moshfegh, A. Z.; Song, Y.-L.; Zhang, H.-L. Unexpected Optical Limiting Properties from MoS_2 Nanosheets Modified by a

Semiconductive Polymer. *Chem. Commun.* **2015**, *51* (61), 12262−12265.
(25) Zhang, J.; Ouyang, H.; Zheng, X.; You, J.; Chen, R.; Zhou, T.; Sui, Y.; Liu, Y.; Cheng, X.; Jiang, T. Ultrafast Saturable Absorption of MoS_2 Nanosheets under Different Pulse-Width Excitation Conditions. *Opt. Lett.* **2018**, *43* (2), 243.
(26) Dhasmana, N.; Fadil, D.; Kaul, A. B.; Thomas, J. Investigation of Nonlinear Optical Properties of Exfoliated MoS_2 Using Photoacoustic Zscan. *MRS Adv.* **2016**, *1* (47), 3215−3221.
(27) Tao, L.; Long, H.; Zhou, B.; Yu, S. F.; Lau, S. P.; Chai, Y.; Fung, K. H.; Tsang, Y. H.; Yao, J.; Xu, D. Preparation and characterization of few-layer MoS2 nanosheets and their good nonlinear optical responses in the PMMA matrix. *Nanoscale* **2014**, *6*, 9713−9719.
(28) Zhou, K.-G.; Zhao, M.; Chang, M.-J.; Wang, Q.; Wu, X.-Z.; Song, Y.; Zhang, H.-L. Size-Dependent Nonlinear Optical Properties of Atomically Thin Transition Metal Dichalcogenide Nanosheets. *Small* **2015**, *11* (6), 694−701.
(29) van Loon, E. G. C. P.; Rösner, M.; Schönhoff, G.; Katsnelson, M. I.; Wehling, T. O. Competing Coulomb and Electron−Phonon Interactions in NbS_2. *npj Quantum Mater.* **2018**, *3* (1), 32.
(30) Maldonado, M.; da Silva Neto, M. L.; Vianna, P. G.; Ribeiro, H. B.; Gordo, V. O.; Carvalho, I. C. S.; de S. Menezes, L.; de Araújo, C. B.; de Matos, C. J. S.; Seixas, L.; Jawaid, A. M.; Busch, R.; Ritter, A. J.; Vaia, R. A.; Gomes, A. S. L. Femtosecond Nonlinear Optical Properties of 2D Metallic NbS_2 in the Near Infrared. *J. Phys. Chem. C* **2020**, *124* (28), 15425−15433.
(31) Kar, I.; Chatterjee, J.; Harnagea, L.; Kushnirenko, Y.; Fedorov, A. V.; Shrivastava, D.; Büchner, B.; Mahadevan, P.; Thirupathaiah, S. Metal-Chalcogen Bond-Length Induced Electronic Phase Transition from Semiconductor to Topological Semimetal in ZrX_2 (X= Se and Te). *Phys. Rev. B: Condens. Matter Mater. Phys.* **2020**, *101* (16), 165122.
(32) Hohenberg, P.; Kohn, W. Inhomogeneous Electron Gas. *Phys. Rev.* **1964**, *136* (3B), B864−B871.
(33) Kohn, W.; Sham, L. J. Self-Consistent Equations Including Exchange and Correlation Effects. *Phys. Rev.* **1965**, *140* (4A), A1133−A1138.
(34) Soler, J. M.; Artacho, E.; Gale, J. D.; García, A.; Junquera, J.; Ordejón, P.; Sánchez-Portal, D. The SIESTA Method for Ab Initio Order- N Materials Simulation. *J. Phys.: Condens. Matter* **2002**, *14* (11), 2745−2779.
(35) Troullier, N.; Martins, J. L. Efficient Pseudopotentials for Plane-Wave Calculations. *Phys. Rev. B: Condens. Matter Mater. Phys.* **1991**, *43* (3), 1993−2006.
(36) Monkhorst, H. J.; Pack, J. D. Special Points for Brillouin-Zone Integrations. *Phys. Rev. B* **1976**, *13* (12), 5188−5192.
(37) Vydrov, O. A.; Van Voorhis, T. Nonlocal van Der Waals Density Functional: The Simpler the Better. *J. Chem. Phys.* **2010**, *133* (24), 244103.

https://dx.doi.org/10.1021/acsphotonics.0c01327
ACS Photonics 2020, 7, 3440−3447